

THESIS FOR THE DEGREE OF LICENTIATE OF ENGINEERING

**Automated Patient-Specific Multi-tissue Segmentation
of MR Images of the Head**

by

KAISER MAHMOOD



CHALMERS

Department of Signals and Systems
CHALMERS UNIVERSITY OF TECHNOLOGY
Gothenburg, Sweden 2013

Gothenburg 2013

Automated Patient-Specific Multi-tissue Segmentation of MR Images of the Head
QAISER MAHMOOD

This thesis has been prepared using L^AT_EX.

Copyright © QAISER MAHMOOD, 2013.
All rights reserved.

Licentiatavhandling vid Chalmers Tekniska Högskola
Ny serie nr R014/2013
ISSN 1403-266X

Department of Signals and Systems
Imaging and Image Analysis Group
Chalmers University of Technology
SE-412 96 Gothenburg, Sweden

Phone: +46 (0)31 772 1716
Fax: +46 (0)31 772 1725
E-mail: qaiserm@chalmers.se

Printed by Chalmers Reproservice
Gothenburg, Sweden, May 2013

To my Parents and Sisters

Abstract

The automated segmentation of magnetic resonance (MR) images of the human head is an active area of research in the field of neuroimaging. The resulting segmentation yields a patient-specific labeling of individual tissues and makes possible quantitative characterization of these tissues (e.g. in the study of Alzheimers disease and multiple sclerosis). The segmentation is also useful for assigning individual tissues conductivity or biomechanical properties for patient-specific electromagnetic and biomechanical simulations respectively. The former are of importance in applications such as EEG (electroencephalography) source localization in epilepsy patients and hyperthermia treatment planning for head and neck tumors. The latter are of interest in applications such as patient-specific motion correction and in surgical simulation.

Automated and accurate segmentation of MR images is a challenging task in the field of neuroimaging because of noise, spatial intensity inhomogeneities, difficulty of MR intensity normalization and partial volume effects (a single voxel represents more than one tissue type). Consequently most of the techniques proposed to date require manual correction or intervention to achieve an accurate segmentation of the brain or whole-head. As a result they are time consuming, laborious and subjective. This thesis presents two automatic and unsupervised segmentation methods, for multi-tissue segmentation of the brain and whole-head respectively from multi-modal MR images, that are more accurate than the state-of-the-art algorithms. The brain segmentation method is based on the mean shift algorithm with a Bayesian-based adaptive bandwidth estimator. The method is called BAMS (Bayesian adaptive mean shift) and can be used to segment the brain into multiple tissue types; e.g. white matter (WM), gray matter (GM) and cerebrospinal fluid (CSF). The accuracy of BAMS was evaluated relative to that of several competing methods using both synthetic and real MRI data. The results show that it is robust to both noise and spatial intensity inhomogeneities compared to competing methods. The whole-head segmentation method is based on a hierarchical segmentation approach (HSA) incorporating the BAMS method. The segmentation performance of HSA-BAMS was evaluated relative to a reference method BET-FAST (based on the BET and FAST tools in the well-known FMRIB Software Library) and three other instantiations of the HSA, using synthetic MRI data with varying noise levels, and real MRI data. The segmentation results show the efficacy and accuracy of proposed method and that it consistently outperforms the BET-FAST reference method. HSA-BAMS was also evaluated indirectly in terms of its impact on the accuracy of EEG source localization using electromagnetic simulations based on a tissue conductivity labeling derived from the segmentation. The results demonstrate that HSA-BAMS outperforms the competing methods, and suggest that it has potential as a surrogate for manual segmentation for EEG source localization.

Preface

This thesis is in partial fulfillment of the requirements for the degree of Licentiate of Engineering at Chalmers University of Technology, Gothenburg, Sweden.

The work herein was jointly undertaken in the Imaging and Image Analysis Group in the Department of Signals and Systems at Chalmers University of Technology, and MedTech West located at Sahlgrenska University Hospital (both in Gothenburg, Sweden) between September 2010 and November 2012. It was performed under the joint supervision of Professor Mikael Persson, Dr. Artur Chodorowski and Assistant Professor Andrew Mehnert. Prof. Persson also acts as examiner of the thesis.

This work has been supported in part by the Chalmers University of Technology and the Higher Education Commission (HEC) of Pakistan. The real data in this thesis was acquired by the Department of Clinical Neurophysiology, Sahlgrenska University Hospital, Gothenburg, Sweden.

List of Publications

This thesis is based on the work contained in the following peer-reviewed papers:

Paper A

Qaiser Mahmood, Artur Chodorowski, Andrew Mehnert, Mikael Persson, "A Novel Bayesian Approach to Adaptive Mean Shift Segmentation of Brain Images", *Proc. of IEEE International Conference on Computer Based Medical Systems (CBMS)*, pp.1-6, Rome, Italy, 20th - 22nd June, 2012.

Paper B

Qaiser Mahmood, Artur Chodorowski, Andrew Mehnert, Johanna Gellermann, Mikael Persson, "Automatic Multi-tissue Segmentation of MR Images of the Head Using a Hierarchical Segmentation Approach Incorporating Bayesian-Based Adaptive Mean Shift", *Submitted to Concepts in Magnetic Resonance Part B: Magnetic Resonance Engineering*.

Paper C

Qaiser Mahmood, Yazdan Shirvany, Andrew Mehnert, Artur Chodorowski, Johanna Gellermann, Fredrik Edelvik, Anders Hedström, Mikael Persson, "On the Fully Automatic Construction of a Realistic Head Model for EEG Source Localization", *Proc. of International Conference of the IEEE Engineering in Medicine and Biology Society (EMBC)*, Osaka, Japan, 3rd - 7th July, 2013.

Other related publications by the author not included in this thesis:

Peer reviewed

1. Yazdan Shirvany, **Qaiser Mahmood**, Fredrik Edelvik, Stefan Jakobsson, Anders Hedström, Mikael Persson, "Non-invasive EEG source localization with Particle Swarm Optimization: Clinical Test". *Submitted to Journal of Biomedical Engineering*.

2. Yazdan Shirvany, Antonio R. Porras, Koushyar Kowkabzadeh, **Qaiser Mahmood**, Hoi-Shun Lui, Mikael Persson, "Investigation of Brain Tissue Segmentation Error and its Effect on EEG Source Localization", *Proc. of International Conference of the IEEE Engineering in Medicine and Biology Society (EMBC)*, pp. 1522-1525, San Diego, USA, 22nd Aug. - 1st Sep., 2012.
3. Yazdan Shirvany, Fredrik Edelvik, Stefan Jakobsson, Anders Hedström, **Qaiser Mahmood**, Artur Chodorowski and Mikael Persson, "Non-invasive EEG source localization with Particle Swarm Optimization: Clinical Test", *Proc. of International Conference of the IEEE Engineering in Medicine and Biology Society (EMBC)*, pp. 6232-6235, San Diego, 22nd Aug. - 1st Sep., 2012.
4. Mikael Persson, Tomas McKelvey, Andreas Fhager, Hoi-Shun Lu, Yazdan Shirvany, Artur Chodorowski, **Qaiser Mahmood**, Fredrik Edelvik, Magnus Thordstein, Anders Hedström, Mikael Elam, "Advances in Neuro Diagnostic Based on Microwave Technology, Transcranial Magnetic Stimulation and EEG source localization", *Proc. of Asia-Pacific Microwave Conference*, Melbourne, Australia, 5th - 8th Dec., 2011.

Not peer reviewed

1. **Qaiser Mahmood**, Artur Chodorowski, Mikael Persson, "Adaptive Segmentation of Brain Tissues from MR Images", *Proc. of Medicinteknikdagarna*, p.86, Linköping, Sweden, 11th - 12th Oct., 2011.
2. **Qaiser Mahmood**, Artur Chodorowski, Andrew Mehnert, Johanna Gellermann, Mikael Persson, "Bayesian Based Adaptive Mean Shift Algorithm for Automatic Multi-Tissue Segmentation of the Human Head", *Proc. of Medicinteknikdagarna*, p.158, Lund, Sweden, 2nd - 3rd Oct., 2012.

Acknowledgments

I would like to express my gratitude to all those who gave me the possibility to complete this thesis.

First of all I would like to thank my supervisor Prof. Mikael Persson for his support throughout the research work and giving the freedom to pursue the research directions I am interested in. I would like to express my deep gratitude to Dr. Artur Chodorowski and Assistant Prof. Andrew Mehnert, my co-supervisors, for their patient guidance, enthusiastic encouragement and useful critiques of this research work. I would like to express my very great appreciation to Dr. Johanna Gellermann for generating real patient ground truth images and also for sharing with me her wide MRI expertise in numerous interesting discussions. I would like also to thank Dr. Fredrik Edelvik from Fraunhofer-Chalmers Research Center and Dr. Yazdan Shirvany for giving me the opportunity to apply this work to the EEG source localization problem in epilepsy. I would like to acknowledge the Department of Clinical Neurophysiology at Sahlgrenska University Hospital, Gothenburg for providing real MR patient data. I extend a special thanks to fellow PhD student Irene Perini for her advice and input on the anatomy of the human head.

I would like to thank all my colleagues at MedTech West and in the Department Signals and Systems at Chalmers University of Technology for their kindness, cooperation, and support. I wish to thank all my friends especially Mats Lindström, Shahid Nawaz, Ramin Moshavegh, Babak Ehteshami and Mohammad Alipoor for their support and creating enjoyable moments in my life. I am grateful to the Higher Education Commission (HEC) of Pakistan and Chalmers University of Technology, Sweden for providing me the scholarship to conduct this research.

Most importantly, none of this would have been possible without the love and patience of my family. I would like to express my heart felt gratitude to my loving parents, brothers and sisters and their families for their support and encouragement.

Qaiser Mahmood, Gothenburg, 2013

Abbreviations and Acronyms

BAMS	Bayesian-Based Adaptive Mean Shift
BET	Brain Extraction Tool
BTSA	Brain Tissue Segmentation Algorithm
COG	Center-Of-Gravity
CSF	Cerebrospinal Fluid
CT	Computed Tomography
DI	Dice Index
EEG	Electroencephalography
FAST	FMRIB's Automated Segmentation Tool
FEHCM	Finite Element Head Conductivity Model
FID	Free Induction Decay
FMRIB	Functional MRI of the Brain
FSL	FMRIB Software Library
GE	Gradient Echo
GM	Gray Matter
GMM	Gaussian Mixture Model
GT	Ground Truth
HMMRF-EM	Hidden Markov Random Field-Expectation Maximization
HSA	Hierarchical Segmentation Approach
IBSR	Internet Brain Segmentation Repository
k NN-AMS	k Nearest Neighbour-Adaptive Mean Shift
LE	Localization Error
MRF	Markov Random Field
MRI	Magnetic Resonance Imaging
MS	Mean Shift
MTSA	Multi-tissue Segmentation Algorithm
NBTSA	Non-Brain Tissue Segmentation Algorithm
NFT	Neuroelectromagnetic Forward Modeling Toolbox
OE	Orientation Error
PD	Proton Density
RE	Relative Error
RF	Radio Frequency
SE	Spin Echo
T1	Longitudinal Relaxation Time
T2	Transverse Relaxation Time
TC	Tanimoto Coefficient
TE	Echo Time
TR	Repetition Time
WM	White Matter

Contents

Abstract	i
Preface	iii
List of Publications	v
Acknowledgments	vii
Abbreviations and Acronyms	ix
Contents	xi
Abbreviations and Acronyms	xii
Part I: Extended Summary	1
1 Introduction	3
1.1 Background and problem definition	3
1.2 Aim and objectives	4
1.3 Scope of the thesis	4
1.4 Overview of the thesis	5
2 Theoretical Background	7
2.1 Anatomy of the human head	7
2.1.1 Brain	8
2.1.2 Non brain	9
2.2 Magnetic Resonance Imaging (MRI)	9
2.2.1 Contrast Mechanisms in MRI	12
2.2.2 Artifacts in MRI	14
2.3 Overview of the basic segmentation techniques underlying existing approaches to brain and whole-head segmentation	15
2.3.1 Mean Shift	15
2.3.2 Segmentation via a hidden Markov random field model (HMRF) and the expectation-maximization (EM) algorithm	19
2.3.3 k -means algorithm	19

2.4	Overview of the segmentation tools used for brain and whole-head segmentation	20
2.4.1	Functional Magnetic Resonance Imaging of the Brain (fMRIB) Software Library (FSL)	20
2.4.2	FreeSurfer	21
2.4.3	Anatomist Software	22
3	Proposed method for brain segmentation	23
3.1	Review of existing brain MRI tissue segmentation methods	23
3.2	New brain MRI tissue segmentation algorithm: Bayesian-based adaptive mean shift (BAMS)	24
3.3	Empirical evaluation of the proposed method	26
4	Proposed method for whole-head segmentation	29
4.1	Review of existing whole-head tissue segmentation methods and tools	29
4.2	New automatic multi-tissue whole-head segmentation algorithm	30
4.3	Empirical evaluation of the proposed method	31
4.4	Indirect evaluation of the proposed method in the context of non-invasive EEG source localization	33
5	Summary of papers and future work	35
5.1	Paper A: A Novel Bayesian Approach to Adaptive Mean Shift Segmentation of Brain Images	35
5.2	Paper B: Automatic Multi-tissue Segmentation of MR Images of the Head Using a Hierarchical Segmentation Approach Incorporating Bayesian-Based Adaptive Mean Shift	35
5.3	Paper C: On the Fully Automatic Construction of a Realistic Head Model for EEG Source Localization	36
5.4	Future work	36
	References	39
	Part II: Publications	43

Part I
Extended Summary

Introduction

1.1 Background and problem definition

Neuroimaging [1] is an important branch of medical imaging. It encompasses a range of techniques used to non-invasively image the brain at all levels of structure and function, ranging from neurotransmitter and receptor molecules to large networks of brain cells. Neuroimaging can be broadly classified into functional imaging and structural imaging.

Functional imaging is used to visualize/assess the neural activity in the brain. The neural activity at a specific location in the brain is associated with localized vascular changes (such as cerebral blood flow) and metabolic changes (such as glucose and oxygen consumption). Functional imaging techniques include positron emission tomography (PET), functional magnetic resonance imaging (fMRI), magnetoencephalography (MEG), and electroencephalography (EEG).

Structural imaging is used to visualize/assess anatomical structures in the brain and the head and to diagnose/characterize tumors and injuries. Structural imaging techniques include X-ray computed tomography (CT) and magnetic resonance imaging (MRI).

Segmentation (i.e. delineation or labeling) of the individual tissues in the structural and functional images makes possible quantitative characterization of anatomical structures as well as diseased tissue and injury. For example the evolution of multiple sclerosis can be monitored in terms of total lesion load determined from a segmentation of the individual lesions in T2-weighted images. Segmentation also makes it possible to assign conductivity or biomechanical properties to the individual tissues for the purpose of constructing electro-conductivity or biomechanical simulations. One approach, known as the finite element method (FEM), involves creating a 3D mesh of simple geometric elements, e.g. tetrahedral elements, from the segmented images. The response of the overall (conductivity or biomechanical) mathematical model is then approximated by the responses of the individual elements in the discrete model.

Electro-conductivity modeling finds use in applications such as non-invasive EEG source localization in epilepsy patients [2], hyperthermia treatment planning for head and neck tumors [3], the study of electric fields induced by transcranial magnetic stimulation (TMS) [4] and the study of deep brain stimulation [5]. Biomechanical modeling finds use in applications such as brain deformation simulation for image-guided neurosurgery [6]

and the study of head trauma in traffic accidents [7].

To date most of the approaches [2, 4, 8] proposed for accurate patient-specific segmentation of the brain or whole-head require manual correction or intervention. Consequently they are time consuming, laborious and subjective. Thus a fully automatic and accurate segmentation method is highly desirable.

1.2 Aim and objectives

The aim of this thesis was to develop fully automatic and accurate patient-specific tissue segmentation methods for both the brain and whole-head using multi-modal MR images (MR images of the same anatomy but acquired using different contrast mechanisms such as T1-weighting, T2-weighting, and proton density weighting). To this end the thesis had the following objectives:

1. To develop an unsupervised method for segmenting the brain into individual tissues.
2. To evaluate the performance of the method using both synthetic and real MR images of the brain.
3. To develop an unsupervised method for segmenting the whole-head into individual tissues.
4. To evaluate the performance of the method using both synthetic and real MR images of the head.

1.3 Scope of the thesis

Only unsupervised image segmentation techniques were considered in this thesis. Such techniques do not require training data but rather explore the intrinsic structure of the image data using various statistics.

Likewise atlas-based segmentation methods (wherein many labeled training images are used to define an atlas) were not investigated. Such methods are not able to handle major structural changes due to pathology (for example, malignant tumor) [9].

The real and synthetic MRI data sets used in this study comprised at most three different MRI modalities. This meant that it was not necessary to perform advanced feature selection and extraction for the purposes of dimensionality reduction.

Only the segmentation of multi-modal MRI data was considered in this thesis. The use of additional imaging modalities, such as X-ray computed tomography or ultrasound, was not investigated.

1.4 Overview of the thesis

The thesis is organized into two main parts.

Part I consists of chapters 2 through 5. Chapter 2 provides the basic anatomical and methodological concepts needed for the remainder of the thesis. The aim and objectives of the thesis are addressed in chapters 3 and 4. Chapter 5 presents a summary of the papers arising from this thesis and discusses future work.

Part II comprises the papers arising from this research.

Theoretical Background

The purpose of this chapter is to acquaint the reader with the basic anatomical and theoretical concepts essential for an understanding of the material presented in subsequent chapters. In particular, the next section presents an overview of the anatomy of the human head, section 2.2 provides an overview of magnetic resonance imaging (MRI), and finally sections 2.3 and 2.4 describe several segmentation techniques and tools underlying existing approaches to brain and whole-head segmentation.

2.1 Anatomy of the human head

This section provides an overview of the anatomy of the human head. The level of detail provided is sufficient for the aim and objectives of this thesis. For a more detailed and comprehensive treatment of the subject, the reader is referred to [10, 11, 12].

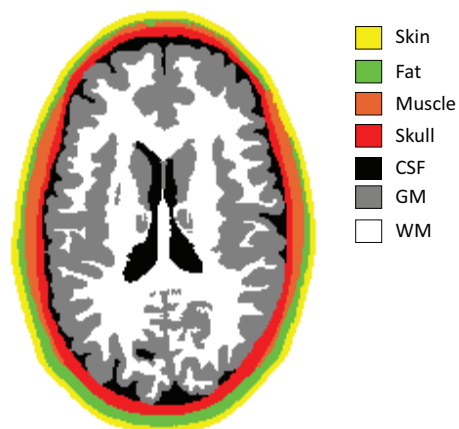


Figure 2.1: Axial slice through the human head showing the major tissue types: white matter (WM) in white, gray matter (GM) in gray, cerebrospinal fluid (CSF) in black, skull in red, fat in green, muscle in brown and skin in yellow.

The human head is made up of several major tissue types as shown in Fig. 2.1. These in turn can be classified as belonging to two major classes: brain and non-brain.

2.1.1 Brain

The human brain is an important part of the central nervous system. Functionally, it can be decomposed into three main parts (see Fig. 2.2).

1. Cerebrum: This is the largest part of the brain and is composed of left and right hemispheres. Each hemisphere can in turn be divided into four lobes:
 - Frontal Lobe: It is involved in functions such as reasoning, planning, parts of speech, voluntary motor function of skeletal muscles, emotions, and problem solving.
 - Parietal Lobe: It is involved in functions such as movement, orientation, recognition, and perception of stimuli.
 - Occipital Lobe: It is involved in visual processing.
 - Temporal Lobe: It is involved in functions such as perception and recognition of auditory stimuli, memory, speech, and smell.
2. Cerebellum: It is located under the cerebrum and is involved in functions such as regulation and coordination of movement, posture, and balance.
3. Brain Stem: It is responsible for regulating breathing, heartbeat, and blood pressure.

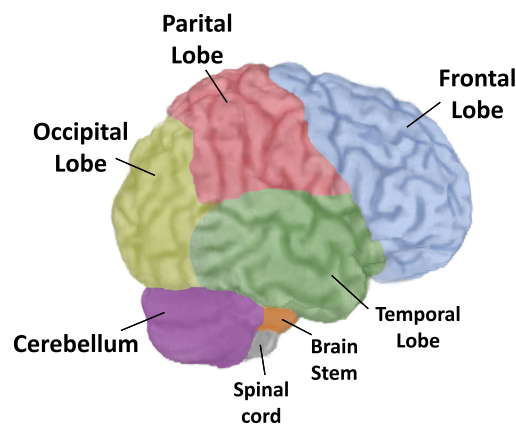


Figure 2.2: Anatomy of the human brain.

Structurally, the brain can be decomposed into three main tissue types (shown in Fig. 2.1):

Gray matter

The gray matter is located on the thin outer layer of the brain, called the cerebral cortex, and also deeper in the brain underneath the white matter. It comprises neuronal cell bodies. Gray matter is involved in various functions including muscle control, speech, emotion, memory, vision and hearing.

White matter

The white matter lies underneath the cerebral cortex and is made up of glial cells and bundles of myelinated axons. The white matter connects various regions of the gray matter, favoring communication between cortical-cortical or cortical-subcortical structures.

Cerebrospinal fluid (CSF)

The CSF is a colorless fluid. It is located in the subarachnoid space (space between the two protective membranes that surround the brain: arachnoid membrane and pia mater), the ventricles (large cavities inside the brain) and the spinal cord. It serves to protect the brain, supply it with nutrition, and to remove waste.

2.1.2 Non brain

The non-brain is composed of four main tissues:

Skull

The skull is a bony structure and has a thickness between 4 to 7 mm. It surrounds the brain, eyes, nose and teeth and serves to protect them.

Skin

The scalp, neck and face surrounding the skull are composed of soft tissue called skin. The skin is made up of two primary layers: epidermis and dermis. The epidermis layer is the outermost layer of the skin and acts as infection barrier. The dermis layer lies underneath the epidermis and provides tensile strength and elasticity to the skin.

Fat

Fat is a soft tissue that lies beneath the skin. It is made up of adipose cells called adipocytes.

Muscle

The term muscle describes another soft tissue located inside the skin. It is composed of protein filaments that slide past one another enabling actions such as eating, blinking and smiling.

2.2 Magnetic Resonance Imaging (MRI)

This section provides a brief overview of the principles of magnetic resonance imaging (MRI). For a more detailed and comprehensive treatment see [13, 14, 15, 16, 17].

MRI is a non-invasive imaging technique. R. Damadian, in 1971, proposed the MRI to use as a medical imaging device. In 2003, P. Lauterbur and P. Mansfield received the Noble prize in Physiology or Medicine for their pioneering work in the development of MRI.

MRI is based on a physical phenomenon called nuclear magnetic resonance which is defined as the ability of magnetic nuclei to absorb energy from an electromagnetic pulse and to radiate this energy back. The hydrogen nucleus or proton is positively charged and possesses an angular momentum called spin. This property causes it to behave as a tiny magnet with a small magnetic field or magnetic moment.

In MR imaging the object to be imaged is placed inside a strong external magnetic field \mathbf{B}_0 that causes the nuclear spins to align along \mathbf{B}_0 with the same orientation (parallel spins) or opposite orientation (anti-parallel spins). The small difference in the two populations yields a bulk magnetization \mathbf{M} , which is the sum of the individual magnetic moments of the individual protons, that depends linearly on the field intensity and is aligned with the \mathbf{B}_0 field (illustrated in Fig. 2.3). This state of magnetization is known as thermal equilibrium.

The magnetization vector \mathbf{M} is the main source of MR signal and is used to produce a MR image. It has two components called longitudinal and transverse magnetization. The longitudinal magnetization (denoted as \mathbf{M}_z) is parallel to the external magnetic field \mathbf{B}_0 while the transverse magnetization (denoted as \mathbf{M}_{xy}) is perpendicular to the \mathbf{B}_0 .

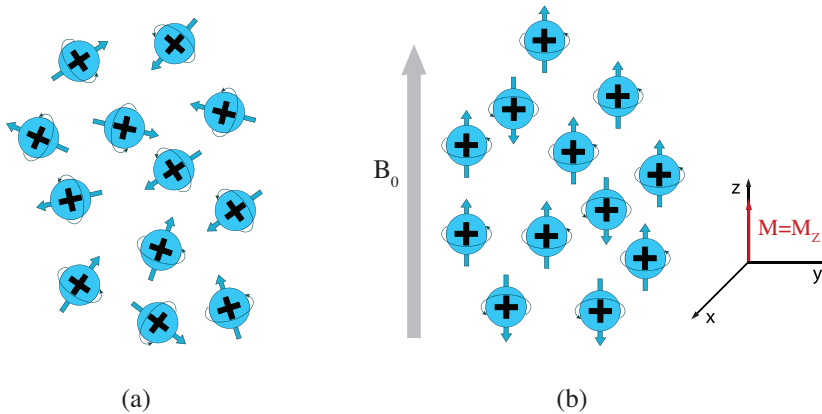


Figure 2.3: Alignment of protons with the \mathbf{B}_0 field: (a) with no external magnetic field, all the protons are oriented randomly (b) in the presence of strong external magnetic field (\mathbf{B}_0), all the protons are aligned (parallel or anti-parallel to external magnetic field \mathbf{B}_0). As a result, a net magnetization $\mathbf{M} = \mathbf{M}_z$ is produced parallel to the external field \mathbf{B}_0 .

When a radio frequency (RF) pulse \mathbf{B}_{RF} (having frequency equal to the Larmor frequency) is applied, it gives energy to the protons. As a result, the magnetization vector \mathbf{M} flips in the transverse plane and the longitudinal component \mathbf{M}_z becomes zero. Once the RF pulse is turned off, another RF signal is generated by the protons due to magnetic resonance phenomena. This signal is decaying towards zero when the magnetization vector $\mathbf{M} = \mathbf{M}_{xy}$ in the transverse plane starts to dephase. This state is known as transverse relaxation or T2-relaxation. The dephasing of \mathbf{M}_{xy} is due to the magnetic moments of protons that are precessing with slightly different frequencies. The decaying signal is known as free induction decay (FID) which is measured by a conductive field coil in the MR

scanner and then it is processed to get the MR image of the object. After T2-relaxation, the protons build up the magnetization vector $\mathbf{M} = \mathbf{M}_z$ again parallel to the original \mathbf{B}_0 field and the state is known as longitudinal relaxation or T1-relaxation. The illustration of T2- and T1-relaxation are shown in Fig. 2.4 and Fig. 2.5 respectively.

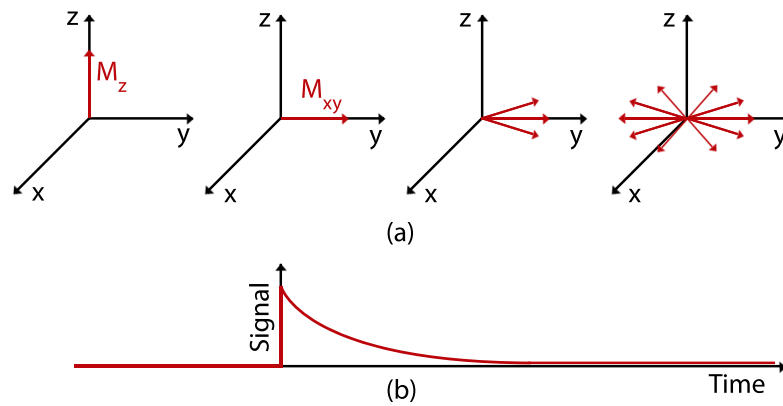


Figure 2.4: T2- relaxation: (a) Dephasing of $\mathbf{M} = \mathbf{M}_{xy}$ in the transverse plane (b) Free induction decay (FID).

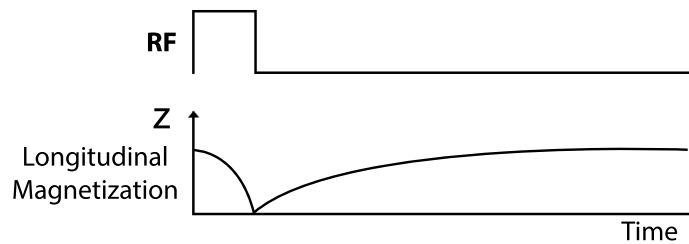


Figure 2.5: T1- relaxation: Application of a perpendicular RF pulse causes longitudinal magnetization $\mathbf{M} = \mathbf{M}_z$ to become zero. Over time, the longitudinal magnetization \mathbf{M}_z will grow back in a direction parallel to the main \mathbf{B}_0 field.

2D and 3D MR imaging

In MRI, the two approaches called 2D and 3D imaging can be used to acquire the image of an object. In 2D imaging, the RF pulse is used to excite only the selected slice of an object. In this way the signal is generated from that particular slice is used to construct the image of that slice. In 3D imaging, the volume of an object that contains the stack of slices is excited with RF pulse to get the image of that particular volume of an object.

2.2.1 Contrast Mechanisms in MRI

In MRI, the contrast between tissues are based on the intrinsic properties of tissues i.e. proton density PD, T1 and T2.

T1 is defined as the time that it takes the longitudinal magnetization M_z to grow back to 63% of its original value. It is related to the rate of regrowth of longitudinal magnetization which is a fundamental source of contrast in T1-weighted images. Different tissues have different rates of T1-relaxation as shown in Fig. 2.6.

T2 is defined as the time that it takes the transverse magnetization M_{xy} to decrease to 37% of its starting value. It is related to the rate of dephasing of transverse magnetization that is a fundamental source of contrast in T2-weighted images. Different tissues have different rates of T2-relaxation as shown in Fig. 2.7.

In the PD-weighted images, the contrast is based on the density of protons in the tissues. Different tissues have different density of protons.

In order to control the weighting amount of T1 and T2 effects in the MR images, the basic imaging parameters are used which are known as echo time (TE) and repetition time (TR). TE is defined as the time between the start of RF pulse and the maximum in the FID response signal. TR is defined as the time between the consecutive RF pulses.

The relative values of TE and TR to produce different contrast weighted image as shown in Fig. 2.8. Herein, T1-weighted image is produced by maximized the T1-relaxation and minimized the T2-relaxation using short TE and intermediate TR. T2-weighted image is produced by maximized the T2-relaxation and minimized the T1-relaxation using long TE and long TR. PD-weighted image is produced by minimized the both T1- and T2-relaxation using short TE and long TR.

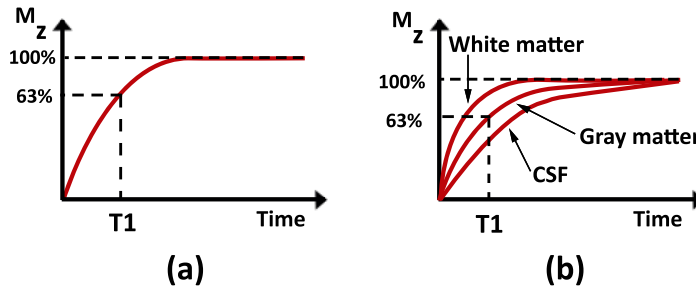


Figure 2.6: (a) T1: longitudinal magnetization increases to 63% of M_z (b) Different tissues have different rates of T1-relaxation.

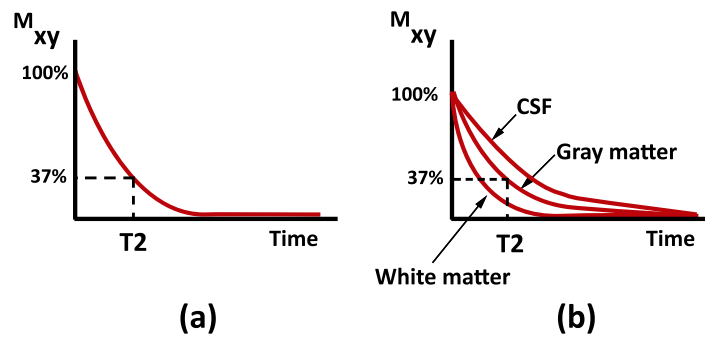


Figure 2.7: (a) T_2 : transverse magnetization decreases to 37% of M_{xy} (b) Different tissues have different rates of T_2 -relaxation.

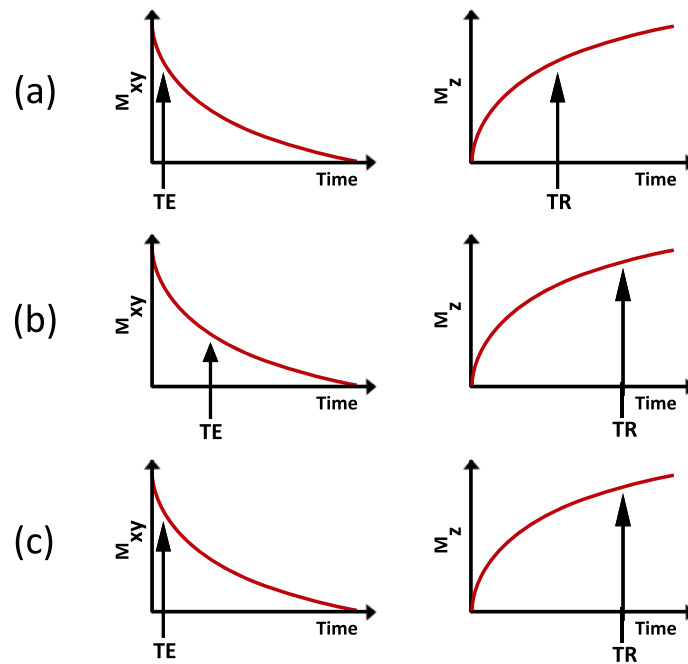


Figure 2.8: Basic imaging parameters: (a) short TE and intermediary TR for T1-weighting (b) long TE and long TR for T2-weighting (c) short TE and long TR for PD-weighting.

Tissues of the human head visualized by magnetic resonance imaging

Fig. 2.9 shows three MR images of the same axial slice through a human head. In these images the contrast between soft tissues can be seen clearly. The contrast in these images are characterised as (a) T1-weighted (b) T2-weighted (c) PD-weighted. In the T1-weighted image the CSF, skull, and fat appear dark and the gray matter, white matter, skin and muscle appear bright. In the T2-weighted image the CSF and skin appear bright, and the skull, fat, muscle, white matter and gray matter appear darker than in the T1-weighted image. In the PD-weighted image the fat, muscle, white matter, gray matter, and CSF appear bright, and the skull appear dark.

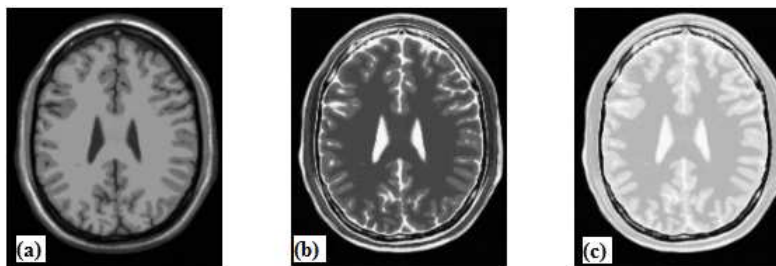


Figure 2.9: Axial slice from an MRI scan of the human head ([18]) (a) T1-weighted (b) T2-weighted (c) PD-weighted image.

Basics pulse sequences for MRI

The two pulse sequences known as spin echo (SE) and gradient echo (GE) are commonly used to generate MR images. These sequences are repeated many times during a scan to generate the image of an object.

In spin echo sequence, a 90° RF pulse is used to flip the magnetization vector \mathbf{M} in the transverse plane. As the protons go through the T1- and T2- relaxation, the transverse magnetization \mathbf{M}_{xy} is gradually dephased. A 180° is applied to rephase it. As a result, a signal (called spin echo) is generated and is used to reconstruct a MR image. In order to generate the different contrast MR images, SE sequence is based on the TE and TR scanning parameters.

In gradient echo sequence, an RF pulse is applied that partly flips the net magnetization vector \mathbf{M} into the transverse plane. A negative gradient pulse is used to dephase the transverse magnetization \mathbf{M}_{xy} and a positive gradient pulse is applied to rephase it. As a result, a signal (called gradient echo) is generated. In GE sequence, the scanning parameters: pulse flip angle, TE, and TR are used to produce different contrast MR images.

2.2.2 Artifacts in MRI

The two major sources of artifacts that degrade the MR image quality significantly and also obfuscate the anatomical and physiological detail are noise and the bias field. The noise in MRI is generally caused by the thermal agitation of electrons in the conductor. It

is usually modeled as Rician distribution [19]. The bias field is a low frequency smooth undesirable signal which is caused by inhomogeneities in the magnetic field of the MR scanner. It changes the intensity values of the image pixels so that the same tissue has different gray level distribution across the image.

2.3 Overview of the basic segmentation techniques underlying existing approaches to brain and whole-head segmentation

Image segmentation refers to the process where every pixel in a digital image is assigned a label and such that pixels sharing the same characteristics are given the same label. Numerous techniques for image segmentation can be found in the literature. No single technique is applicable for all problems and no general theory exists for synthesizing a segmentation solution for any given problem. The image analysis practitioner must therefore devise solutions based on one or more techniques and using experience and trial and error.

In this section we give a brief description of the elementary segmentation techniques used in the brain and whole-head segmentation methods presented/discussed in later chapters.

2.3.1 Mean Shift

Mean shift is a non-parametric mode seeking and clustering technique originally proposed for the analysis of data by Fukunaga and Hostetler [20]. Its application to image processing and computer vision tasks such as filtering, image segmentation and real time object tracking was pioneered by Comaniciu et al. [21].

Mean shift does not require any prior information concerning the number of clusters, and does not constraint the size or shape of the clusters. Mean shift clustering is based on an adaptive gradient ascent approach to estimate the local maxima or modes of multivariate distributions underlying the feature space. Ultimately each feature point is associated with a mode thereby defining clusters. The basic principle of mean shift clustering is described below.

Let $\{\mathbf{x}_i \in \mathbb{R}^d | i = 1 \dots n\}$ denote a set of feature vectors (data points) in d - dimensional space. The kernel density estimate of the underlying multivariate probability function at point \mathbf{x} is given by

$$\hat{f}_K(\mathbf{x}) = \frac{1}{n} \sum_{i=1}^n |\mathbf{H}|^{-1/2} K(|\mathbf{H}|^{-1/2}(\mathbf{x} - \mathbf{x}_i)) \quad (2.1)$$

where \mathbf{H} is a $d \times d$ symmetric positive definite bandwidth matrix. For a radially symmetric kernel, $\mathbf{H} = h^2 \mathbf{I}$ which leads to

$$\hat{f}_K(\mathbf{x}) = \frac{c_{k,d}}{nh^d} \sum_{i=1}^n k\left(\left\|\frac{\mathbf{x} - \mathbf{x}_i}{h}\right\|^2\right) \quad (2.2)$$

where $h > 0$ is a scalar bandwidth and $k : [0, 1] \rightarrow \mathbb{R}$ is the kernel profile of the radially

symmetric kernel K with bounded support defined as

$$K(\mathbf{x}) = c_{k,d}k\left(\|\mathbf{x}\|^2\right) \quad \|\mathbf{x}\| \leq 1 \quad (2.3)$$

and $c_{k,d}$ is a normalizing constant ensuring that the kernel K integrates to 1. The typical kernels used in the mean shift applications are Gaussian K_G and Epanechnikov K_E given as

$$K_G(\mathbf{x}) = c_{k,d}k_G = c_{k,d}\exp\left(-\frac{1}{2}\|\mathbf{x}\|^2\right) \quad (2.4)$$

$$K_E(\mathbf{x}) = c_{k,d}k_E = c_{k,d}(1 - \|\mathbf{x}\|^2) \quad \|\mathbf{x}\| \leq 1 \quad (2.5)$$

where k_G and k_E are the kernel profiles of K_G and K_E respectively. The derivative of the sample point density estimator in eq. 2.2 leads to

$$\begin{aligned} \hat{\nabla} f_K(\mathbf{x}) &\equiv \nabla \hat{f}_K(\mathbf{x}) = \frac{2c_{k,d}}{nh^{d+2}} \sum_{i=1}^n (\mathbf{x} - \mathbf{x}_i) k' \left(\left\| \frac{\mathbf{x} - \mathbf{x}_i}{h} \right\|^2 \right) \\ &= \frac{2c_{k,d}}{nh^{d+2}} \left[\sum_{i=1}^n g \left(\left\| \frac{\mathbf{x} - \mathbf{x}_i}{h} \right\|^2 \right) \right] \times \left[\frac{\sum_{i=1}^n \mathbf{x}_i g \left(\left\| \frac{\mathbf{x} - \mathbf{x}_i}{h} \right\|^2 \right)}{\sum_{i=1}^n g \left(\left\| \frac{\mathbf{x} - \mathbf{x}_i}{h} \right\|^2 \right)} - \mathbf{x} \right] \end{aligned} \quad (2.6)$$

where $g(x) = -k'(x)$. The right-most factor (in square brackets) in eq. 2.6 is called the mean shift vector. It points toward the direction of maximum increase in density and also provides the basis for clustering. The mean shift vector can be written as

$$M_{h,G}(\mathbf{x}) = \frac{\nabla \hat{f}_K(\mathbf{x})}{\hat{f}_G(\mathbf{x})} = \frac{\sum_{i=1}^n \mathbf{x}_i g \left(\left\| \frac{\mathbf{x} - \mathbf{x}_i}{h} \right\|^2 \right)}{\sum_{i=1}^n g \left(\left\| \frac{\mathbf{x} - \mathbf{x}_i}{h} \right\|^2 \right)} - \mathbf{x} \quad (2.7)$$

where G represents the kernel and defined as

$$G(\mathbf{x}) = c_{g,d}g(\|\mathbf{x}\|^2) \quad (2.8)$$

The kernel G starts from an initial position \mathbf{y}_1 and moves towards the position closer to the higher density region. The update rule of kernel position is given by

$$\mathbf{y}_{j+1} = \frac{\sum_{i=1}^n \mathbf{x}_i g \left(\left\| \frac{\mathbf{y}_j - \mathbf{x}_i}{h} \right\|^2 \right)}{\sum_{i=1}^n g \left(\left\| \frac{\mathbf{y}_j - \mathbf{x}_i}{h} \right\|^2 \right)}, \quad j = 1, 2, \dots \quad (2.9)$$

where $\{\mathbf{y}_j\}_{j=1,2,\dots}$ represents the successive locations of the kernel G . The characteristics of convergence for the discrete data depends on the employed kernel. The guaranteed convergence of the mean shift algorithm to the local maximum of a probability density function, is achieved due to the adaptive magnitude of the mean shift vector $M_{h,G}(\mathbf{x})$. In a lower density region, the magnitude of $M_{h,G}(\mathbf{x})$ is large, and in a high density region

(i.e. closer to a mode), the magnitude is small. The feature (data) points that converge to the same mode constitute a cluster. An example of mean shift (MS) clustering for 2D intensity feature space is illustrated in Fig. 2.10.

MS can be applied for image segmentation where the feature space is extended by concatenating the spatial coordinates of a pixel with its intensity (range) value. An image is represented as a 2D or 3D lattice of d -dimensional intensity vectors (pixels). The space of the lattice is called the spatial domain while the space of intensity vectors is called the range domain. To perform image segmentation using MS in the joint spatial-range domain, a joint spatial-range domain kernel $K_{h_s, h_r}(\mathbf{x})$ is used. It is defined as a product of spatial and range domain kernels and is given by

$$K_{h_s, h_r}(\mathbf{x}) = \frac{C}{h_s^p h_r^d} k\left(\left\|\frac{\mathbf{x}^s}{h_s}\right\|^2\right) k\left(\left\|\frac{\mathbf{x}^r}{h_r}\right\|^2\right) \quad (2.10)$$

where \mathbf{x}^s represents a vector of pixels spatial coordinates, \mathbf{x}^r represents a vector of pixels range (intensity) values and h_s and h_r are their corresponding kernel bandwidths, and C is a normalization constant.

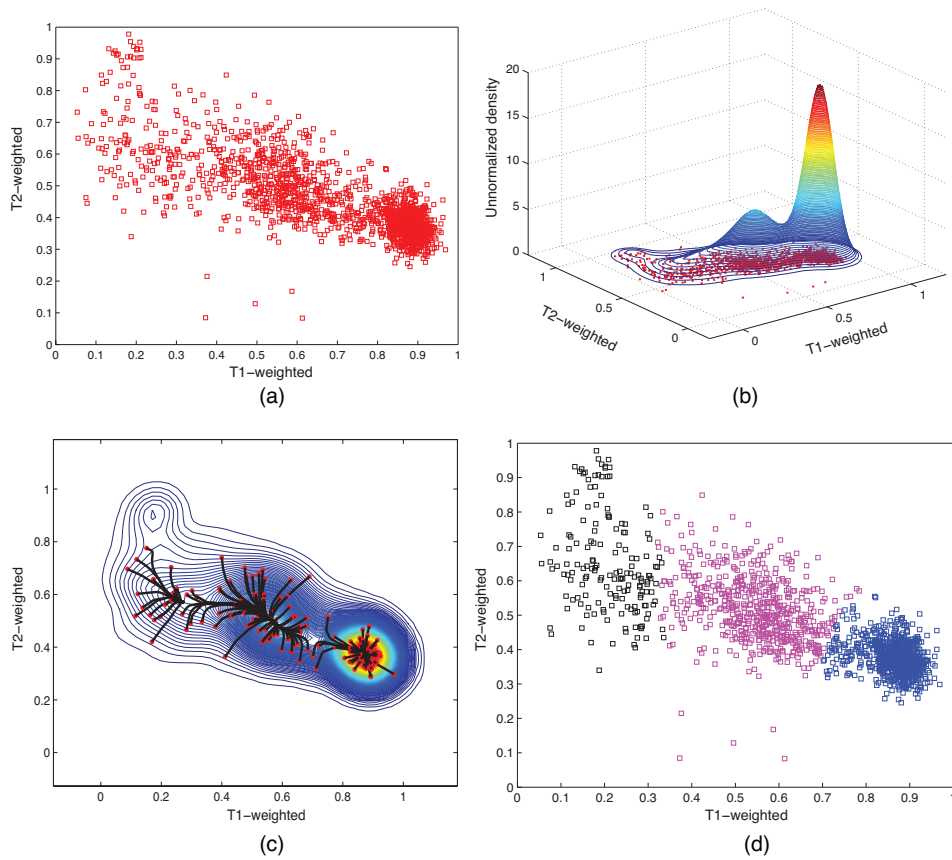


Figure 2.10: (a) The 2D intensity feature space for data from a multi-modal MR image (T1- and T2-weighted) of the brain of a volunteer (b) Density estimate for the 2D intensity feature space (using a Gaussian kernel with bandwidth $h=0.08$) (c) Mean shift procedure trajectories for some feature points drawn over the Gaussian density estimate (d) Resulting clusters after applying mean shift (CSF in black, gray matter in magenta and white matter in blue).

2.3.2 Segmentation via a hidden Markov random field model (HMRF) and the expectation-maximization (EM) algorithm

The hidden Markov random field model and expectation maximization (HMRF-EM) framework is an unsupervised parametric method initially proposed by Zhang et al. [22] for the segmentation of brain tissues in MR images. In the HMRF-EM framework, HMRF is a stochastic model generated by a Markov random field (MRF) whose state sequence is estimated indirectly through observations. The advantage of HMRF is derived from the MRF theory in which the spatial information of an image is encoded through contextual constraints of neighbouring pixels. The EM algorithm is used to fit this model. The principle of the HMRF-EM method is described below.

Let $\mathbf{y} = (y_1, \dots, y_N)$ represent a gray-scale image such that y_i represents the intensity of the i -th pixel. Let $\mathbf{x} = (x_1, \dots, x_N)$ represent a label image such that $x_i \in L$ is the label corresponding to pixel y_i and L is the set of all possible labels.

According to the maximum a posteriori (MAP) criterion, the optimal labeling $\hat{\mathbf{x}}$ is obtained as follows

$$\hat{\mathbf{x}} = \arg \max_{\mathbf{x}} \{P(\mathbf{y}, \Theta | \mathbf{x}) P(\mathbf{x})\} \quad (2.11)$$

where \mathbf{x} is a realization of an MRF and $P(\mathbf{x})$ is its prior probability given by

$$P(\mathbf{x}) = Z^{-1} \exp(-U(\mathbf{x})) \quad (2.12)$$

where Z is a normalizing constant and $U(\mathbf{x})$ is an energy function. $P(\mathbf{y}, \Theta | \mathbf{x})$ represents the joint likelihood probability and is defined

$$P(\mathbf{y} | \mathbf{x}, \Theta) = \prod_i P(y_i | x_i, \theta_{x_i}) \quad (2.13)$$

where $P(y_i | x_i, \theta_{x_i})$ is a Gaussian distribution with parameters $\theta_{x_i} = \{\mu_{x_i}, \sigma_{x_i}\}$. $\Theta = \{\theta_l | l \in L\}$ is the set of parameters which are estimated using the EM algorithm. In [22], the iterated conditional modes (ICM) algorithm [23] (one of the optimization methods) is used to obtain the optimal solutions of MAP.

2.3.3 k -means algorithm

The term k -means was introduced by MacQueen [24] in 1967 to describe one of the simplest unsupervised clustering algorithms. In this algorithm, the partitioning of n data points into k disjoint subsets S_j is done by minimizing the following cost function

$$J = \sum_{j=1}^k \sum_{\mathbf{x}_i \in S_j} \|\mathbf{x}_i - \mu_j\|^2. \quad (2.14)$$

where \mathbf{x}_i is a vector representing the i th data point and μ_j is the centroid of the data points in S_j .

The standard k -means algorithm starts with random initialization of k centroids. Each data point is then assigned to a closest centroid and the number of data points closest to a centroid form a cluster. The new centroid is computed according to the data points in the cluster. This process is continued until the data points stop changing their centroids or clusters. The downside of this algorithm is that it is quite sensitive to the initialization of the centroids of the clusters and it provides clustering in the intensity (range) domain only.

Different variations of k -means algorithm can be found in [9, 25] that are applied for the brain tissue segmentation. Herein, we give a short description of these algorithms which are presented in the later chapters.

Tree structure k -means (tskmeans) algorithm

To avoid the initialization problem, the tree structure k -means (tskmeans) algorithm [25] begins with one cluster and then the clusters grow in a tree until the desired number of clusters is obtained. At each step, the resulting cluster or tree node is split into two more clusters for the next stage.

Voxel-weighted k -means algorithm

In voxel-weighted k -means algorithm [9], the centroid is defined as

$$\mu_j = \sum_{\mathbf{x}_i \in \mathbf{I}_m, \forall \mathbf{I}_m \in S_j} w_m \cdot \mathbf{I}_m \quad (2.15)$$

where the intensity vector \mathbf{I}_m , for each mode m is assigned to class j , is weighted by w_m , the relative portion of the total number of data points (voxels) it represents.

2.4 Overview of the segmentation tools used for brain and whole-head segmentation

Herein, we give a brief description of segmentation tools used for the brain and whole-head segmentation that are presented/discussed in later chapters.

2.4.1 Functional Magnetic Resonance Imaging of the Brain (FMRIB) Software Library (FSL)

FSL [26] is a software devolved and maintained by the Functional Magnetic Resonance Imaging of the Brain (FMRIB) analysis group in Oxford University, UK. It contains a comprehensive library of analysis tools for structural MRI head/brain imaging data. The tools provided for MRI head/brain segmentation are as follows.

FMRIB's Automated Segmentation Tool (FAST)

The FAST tool is used to segment the 3D image (stack of MR slices) of the brain into different tissue types (gray matter, white matter, CSF, etc.). The underlying method is based on the HMRF-EM method described in section 2.3.2.

Brain Extraction Tool (BET)

The BET tool [27] is used to segment the brain, skull, and skin. The underlying methods used in the tool are described below.

1. A rough threshold for the brain matter/background is estimated by computing the global minimum and maximum intensity of an image using the intensity histogram. The minimum intensity lies at the 2% of the cumulative histogram and the maximum intensity lies at 98% of the cumulative histogram. The rough threshold for the brain matter/background lies 10% of the way between minimum and maximum intensity of the image.
2. In the second step, this rough threshold is used to estimate the position of centre-of-gravity (COG) of the brain/head in the image. This COG is computed by average of all voxels positions that have intensity greater than rough threshold.
3. Then a rough radius of brain/head is estimated by counting all voxels with intensity greater than rough threshold. This radius is used for initializing the surface model.
4. Next a triangular tessellation (mesh) of the spherical surface is initialized whose center is at the COG and radius is equal to half of the estimated rough brain/head radius. The surface model is basically a deformable model [28] and it is deformed inside the head until the brain's boundary is detected. The surface model is stopped at the surface of brain where the intensity of the voxels less than the local threshold. The local threshold distinguishes the brain from the non-brain tissue. It is based on both the local maximum and global minimum thresholds of the image and a user-defined input parameter called the fractional constant.
5. Finally, the surfaces of non-brain tissue: skull and skin are extracted by searching the minimum and maximum intensity through a line (pointed outwards) perpendicular to the brain surface.

2.4.2 FreeSurfer

The software, FreeSurfer [29] is developed by the Laboratory for Computational Neuroimaging at the Martinos Center for Biomedical Imaging. It is a set of tools for analysis and visualization of structural and functional brain imaging data. In FreeSurfer, the tool used for the whole-brain segmentation is based on the segmentation method that includes registration of brain atlas, framework of Bayesian estimation theory, Markov random field (MRF) spatial model and ICM algorithm [23]. The Bayesian framework allows to incorporate the prior information about the spatial distribution of individual brain structures and their expected intensity appearance through atlas. The ICM is applied to estimate the optimal labelling of voxels. MRF is used to model the neighbouring voxels interaction in order to improve the segmentation smoothness.

2.4.3 Anatomist Software

The Anatomist¹ software interactive tools for segmenting the brain imaging data. These tools need expert or clinician (who are good in anatomical knowledge) interaction for generating manual labelling of brain/head tissues.

¹www.brainvisa.info

Proposed method for brain segmentation

This chapter addresses objectives 1 and 2 of this thesis described in chapter 1. It consists of three sections. Section 3.1 presents a review of existing methods for brain tissue segmentation. The proposed method is then presented in section 3.2. Finally, an empirical evaluation of the proposed method is presented in section 3.3.

3.1 Review of existing brain MRI tissue segmentation methods

A wide range of brain MRI tissue segmentation methods have been proposed in the literature. A recent review of such methods can be found in [30]. Two brain MRI segmentation methods published since this review are [31, 32]. More reviews of MR brain image segmentation methods can be found in [33] and [34]. From the machine learning point of view these methods can be broadly classified into supervised and unsupervised methods.

Supervised segmentation methods [33, 35] require prototypes, such as the intensity values of labeled voxel samples, from each tissue type to train a classifier. This classifier is then used to label unseen voxels. Artificial neural networks and k NN classifiers are the two examples of supervised segmentation methods. A downside of these methods that they require accurate labeled tissues as training data to train their classifier for the tissue segmentation.

Unsupervised methods don't require any labeled data sets. Parametric methods are one of the unsupervised methods. These methods assume some distributional form for the underlying probability distribution of the data and seek to estimate its parameters. KVL (K. Van Leemput) [36], CGMM (Constrained Gaussian mixture model) [37], AMAP (Adaptive maximum a posteriori probability map) and BMAP (Biased maximum a posteriori probability map) [25] are examples of such methods. In these methods, the voxel intensities are modeled by a Gaussian mixture model (GMM) which is a weighted sum of k component Gaussian densities (usually k is 3 or more). A GMM is parameterized by the mean vectors, covariance matrices and mixture weights from all component densities and these parameters are estimated using the Expectation-Maximization (EM) algorithm. The final segmentation is done by assigning every voxel to the tissue type for which it has the highest *a posteriori* probability. A drawback with these approaches is that they may give poor tissue classifications in the presence of additive noise and the multiplicative

bias field [9]. Another parametric approach, which is regarded as a state-of-the-art algorithm, is MPM-MAP (maximizer of the posterior marginals-maximum a posteriori) [38]. This algorithm is based on non-rigid registration of the brain atlas and uses expectation-maximization (EM) for estimation of the model parameters and Markov Random Fields (MRF) for spatial coherences. A downside of this approach is that it involves two critical steps for accurate segmentation of brain tissues. First it requires appropriate atlas which doesn't always exist for the data at hand (for example, brain data obtained from young infants and brain data with tumors). The second is the implementation of MRF algorithm which is computationally expensive and require critical parameters settings at higher dimensional feature space [9].

An alternative unsupervised approach that doesn't require many parameters, incorporates the spatial information easily into a higher dimensional feature space (multi-modal MR images) without using a MRF model, is mean shift (MS) clustering (described in section 2.3.1). Mean shift clustering is one of the non-parametric approaches. In this approach, only the kernel size influences the clustering which is called bandwidth. A couple of MS methods [9, 39] based on the adaptive bandwidth have been proposed for brain tissue segmentation in MR images. The adaptive bandwidth estimator [21] used in [9], is based on the k nearest neighbour (k NN) distance. A downside is that this approach is known to be biased by outliers for Euclidean distance [40]. Drawback of adaptive bandwidth estimator used in [39] include that it requires an initial density estimate (called the pilot estimate). These collective limitations motivated the development of new algorithm presented in the next section. The algorithm employs an adaptive approach based on a novel variation on the Bayesian approach initially proposed in [40] for the estimation of a global fixed kernel bandwidth.

3.2 New brain MRI tissue segmentation algorithm: Bayesian-based adaptive mean shift (BAMS)

Our novel brain MRI tissue segmentation algorithm is called Bayesian-based adaptive mean shift (BAMS). The method is described briefly below.

BAMS is a variation on the k NN-AMS (adaptive mean shift) segmentation framework of Mayer and Greenspan [9]. The fundamental difference is that BAMS is based on a Bayesian adaptive bandwidth estimator instead of a k NN adaptive bandwidth estimator.

In BAMS, the bandwidth is modeled by the *a posteriori* probability density function $p(s|\mathbf{x})$ of local data spread s given the data point \mathbf{x} . Let $M < n$ (total number of data points) be the number of nearest neighborhoods to a data sample \mathbf{x}_i . The evaluation of probabilities over the entire set of neighborhoods M_j is given as

$$P(s|\mathbf{x}_i) = \int P(s|M_j, \mathbf{x}_{M_j})P(M_j|\mathbf{x}_{M_j})dM_j \quad (3.1)$$

Bayes rule yields

$$P(M_j|\mathbf{x}_{M_j}) = \frac{P(\mathbf{x}_{M_j}|M_j)P(M_j)}{P(\mathbf{x}_{M_j})} \quad (3.2)$$

where $P(\mathbf{x}_{M_j}|M_j)$ is the probability of the data sample \mathbf{x}_{M_j} given the M_j nearest neighborhood and $P(M_j)$ is a uniform distribution.

For a given M_j the local variance s_j is computed as

$$s_j = \sum_{l=1}^{M_j} \frac{\|\mathbf{x}_{(i,l)} - \mathbf{x}_i\|^2}{M_j - 1} \quad i = 1, 2, \dots, n, j = 1, 2, \dots, N \quad (3.3)$$

where $\mathbf{x}_{(i,l)}$ is the l -th nearest neighbor to the data point \mathbf{x}_i . The distribution of variances is modeled as the Gamma distribution defined as

$$P(s|\alpha, \beta) = \frac{s^{\alpha-1}}{\beta^\alpha \Gamma(\alpha)} e^{-\frac{s}{\beta}} \quad s \geq 0, \alpha, \beta > 0 \quad (3.4)$$

where α and β define the shape and the scale of the Gamma distribution, respectively [40].

Finally the adaptive bandwidth is estimated by the product of these parameters, identically the mean of the Gamma distribution. Fig. 3.1 illustrates this bandwidth estimation approach for a data point \mathbf{x}_i (the data originates from synthetic multi-modal MR images).

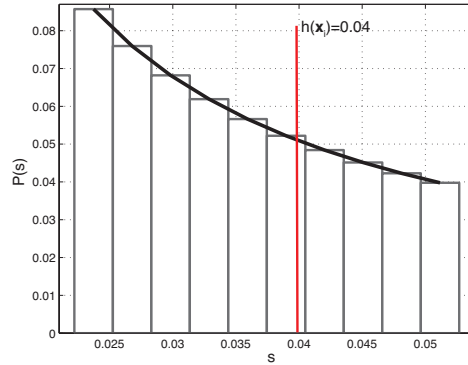


Figure 3.1: Illustration of bandwidth estimation (shown in red) for a data point \mathbf{x}_i . Histogram of local neighborhood variances s fitted to the Gamma distribution $P(s)$.

After estimating the bandwidth h_i for each feature point, the fixed bandwidth h is replaced by h_i in eq. 2.9 (as described in mean shift algorithm in section 2.3.1) to achieve the clustering of the brain/non-brain tissues. The output of the adaptive MS is a set of clusters. The clusters which are close to one another (with respect to the Mahalanobis distance) in the range domain (decided using a window of radius R) are then pruned. The pruning is done in an iterative fashion with increasing R until the variance of merging clusters reaches a preset threshold value. Finally, the desired number of tissues in the brain/non-brain is obtained by applying voxel-weighted k -means algorithm (discussed in section 2.3.3) [9].

3.3 Empirical evaluation of the proposed method

This section summarizes the empirical evaluation, detailed in paper A, of the proposed method. The evaluation was performed using multimodal (T1-, T2-, and PD-weighted) synthetic MRI data with differing noise levels (downloaded from the Brainweb [18]), and also T1-weighted images of 20 normal subjects with varying spatial inhomogeneities downloaded from the IBSR (Internet Brain Segmentation Repository) [41]. Refer to paper A for more details concerning this data. The quantitative and qualitative performance of the proposed method BAMS was evaluated relative to k NN-AMS (our own implementation) and several competing methods (AMAP, BMAP and tsk -means (tree structure k -means) [25]).

Quantitative results

The quantitative results of multi-modal synthetic MR volume (containing six slice) (see Fig. 1 in paper A) shows that BAMS outperforms the k NN-AMS for the gray matter (GM) and CSF classification for the noise levels 5% and 9%. It also outperforms k NN-AMS for the white matter (WM) classification for the noise level 7%.

Herein, we present quantitative results of 20 real T1-weighted brain volumes in detail that are summarized in Table 2 in paper A. The quantitative results (Tanimoto coefficient) for each T1-weighted brain volume for each tissue type are shown in Fig. 3.2. It can be seen that the proposed method BAMS outperforms AMAP, BMAP and tsk -means for each tissue classification in the first five volumes. These volumes are acknowledged in the literature [9] as difficult to segment due to low contrast and high spatial inhomogeneities. It can also be observed that the performance of proposed method is closer to or better than k NN-AMS method across the range of T1-weighted brain volumes for each tissue classification.

Qualitative results

The qualitative results for both multi-modal synthetic and real T1-weighted MR images (see Fig. 3 and Fig. 4 in paper A) show that k NN-AMS misclassifies CSF more frequently than BAMS.

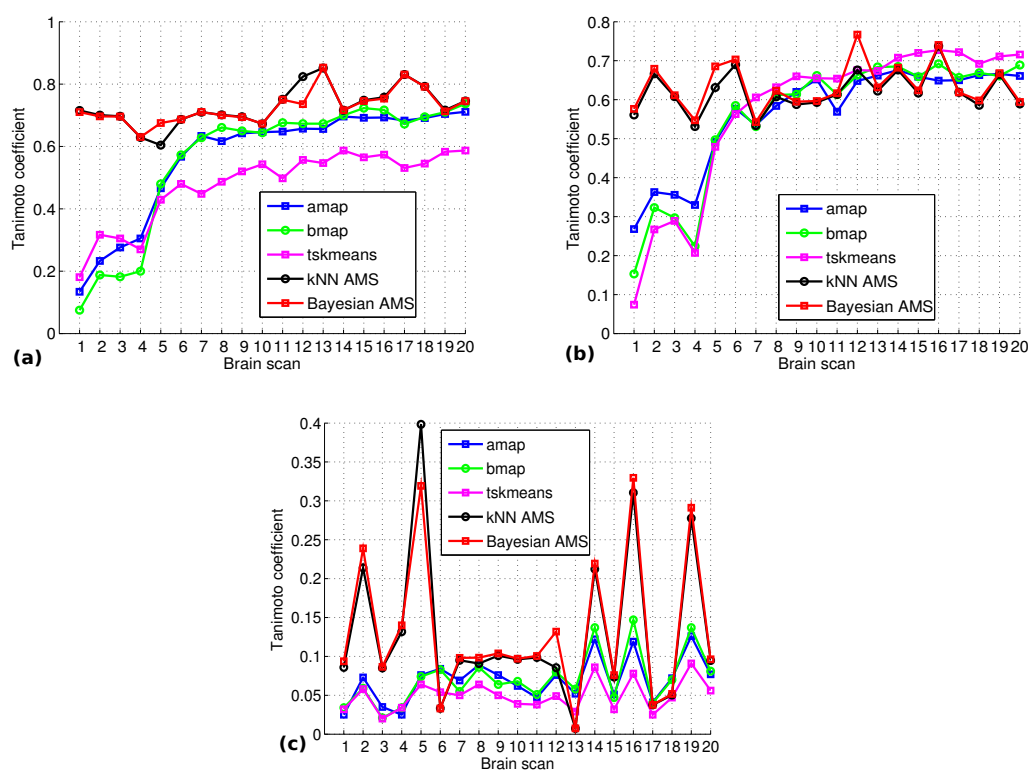


Figure 3.2: (a) WM (top left), (b) GM (top right), (c) CSF (bottom center) (Methods: BAMS is shown in red, k NN-AMS in black, AMAP in blue, BMAP in green and tsk -means in magenta. In plots, along the horizontal axis, the real T1-weighted brain volumes (Brain scans) are ordered in decreasing level of difficulty (low contrast and high spatial inhomogeneities).

Proposed method for whole-head segmentation

This chapter addresses objectives 3 and 4 of this thesis described in chapter 1. It includes four sections. Section 4.1 presents a review of existing methods and tools for whole-head tissue segmentation. The proposed method is then presented in section 4.2. An evaluation of the segmentation accuracy of the proposed method is presented in section 4.3. Finally section 4.4 presents an indirect evaluation of the proposed method in the context of EEG source localization.

4.1 Review of existing whole-head tissue segmentation methods and tools

To date only a couple of methods have been proposed for automated whole-head segmentation. Dokládal et al. [42] proposed an automatic method based on mathematical morphology operators. Amato et al. [43] proposed a non-parametric discriminant analysis method for automatic multi-modal MR head segmentation. This method requires training data to learn the density functions of the individual tissues. The former algorithm has downside that it applies only on single T1-weighted images and the latter has limitation that it needs correctly labeled tissues as training data to train their classifier for the tissue segmentation.

Several neuroscience application-based papers proffer semi-automatic whole-head segmentation approaches based on freely available software such as FSL [26], Anatomist and FreeSurfer [29]. For example, Rullmann et al. [2] used FSL together with the Anatomist software in a two-step process to segment the whole-head of an epilepsy patient from T1-weighted images. In the first step the FSL tool BET (described in section 2.3.4) [22, 27] was used to segment the head into brain, skin and skull tissues and then the segmentation result was manually corrected using the Anatomist software. In the second step the brain tissue was further segmented into cerebrospinal fluid (CSF), white matter (WM) and gray matter (GM) using the Anatomist software. The final segmentation was then used to construct a conductivity model for EEG source localization. Another example, Optiz et al. [4] used FreeSurfer and FSL to segment the whole-head of a healthy subject using T1- and T2-weighted images. In particular FreeSurfer was used to segment the GM and WM surfaces using the T1-weighted images, and the BET tool used

to segment the CSF, skin and skull surfaces. The quality of the initial surface meshes was then semi-automatically corrected and used to construct a conductivity volume for studying the fields induced by transcranial magnetic stimulation (TMS). The drawback to these semi-automatic methods is that they are time consuming, laborious and subjective. Most recently Zynep [44] introduced a new toolbox called Neuroelectromagnetic forward modeling toolbox (NFT) for generating realistic head models from T1-weighted image and for solving the forward problem of electro-magnetic source imaging numerically. In NFT, the segmentation tool is based on thresholding, morphological operations, and the watershed transform to segment the whole-head into four tissues: brain, CSF, inner skull and outer skull. A downside to this tool is that it requires expert intervention for providing the seeds for accurate segmentation of brain and outer skull.

The drawbacks of the existing automatic and semi-automatic methods outlined above served as the motivation for the development of a new fully automatic and accurate method for multi-tissue segmentation of multi-modal MR images of the head presented in the next section.

4.2 New automatic multi-tissue whole-head segmentation algorithm

Our proposed method is based on a hierarchical segmentation approach (HSA) incorporating our novel Bayesian-based adaptive mean shift (BAMS) segmentation algorithm introduced in Chapter 3. We call this method HSA-BAMS. In common with several semi-automatic approaches in the literature, the HSA involves initially segmenting the data into brain tissue and non-brain tissue sub-volumes. The idea here is that the detection of brain and non-brain tissue is a much simpler problem than the problem of segmenting each of these into multiple tissue classes. What distinguishes our HSA is that a single method is proposed for segmenting the brain tissue and non-brain tissue sub-volumes into multiple tissue classes; in particular BAMS in the case of HSA-BAMS.

Proposed Hierarchical Segmentation Approach (HSA)

The proposed HSA takes as input one or more pre-processed and spatially co-registered sets of MR images of the whole head. Collectively this data can be considered a single spatial volume (V) with vector-valued voxels. This volume is segmented into two disjoint sub-volumes, brain tissue (V_{BT}) and non-brain-tissue (V_{NBT}), using a brain tissue segmentation algorithm (BTSA) and a non-brain tissue segmentation algorithm (NBTSA) respectively. Finally the multi-tissue segmentation algorithm (MTSA) is applied independently to the V_{BT} and V_{NBT} volumes to segment them into individual tissue classes V_{BT_1} , V_{BT_2}, \dots and V_{NBT_1} , V_{NBT_2}, \dots respectively. The schematic diagram of our proposed HSA is shown in Fig. 4.1.

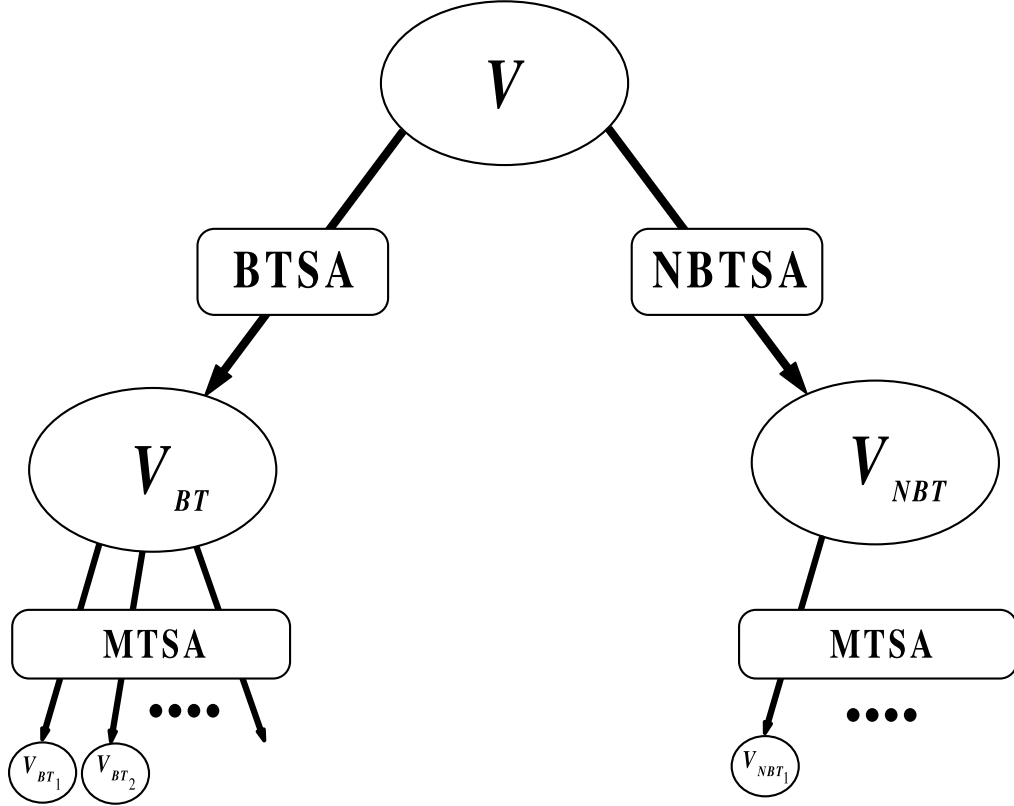


Figure 4.1: Schematic of the proposed method HSA for automated whole-head segmentation.

4.3 Empirical evaluation of the proposed method

This section summarizes the empirical evaluation, detailed in paper B, of the proposed method, HSA-BAMS. The evaluation was performed using three MRI data sets: (1) multi-modal (T1-, T2-, and PD-weighted) synthetic data with differing noise levels (obtained from the Brainweb [18]), (2) T1-weighted data from a healthy volunteer and (3) multi-modal (T1- and T2-weighted) data from second healthy volunteer (acquired on a 3T Philips Achieva scanner at Sahlgrenska University Hospital, Gothenburg, Sweden). The details of these MR data sets are described in paper B.

Ground truth for the synthetic data was obtained from the nine tissue classes defined in the labeled data obtained from Brainweb. This was reduced to seven classes by merging the connective and skin tissue classes, and the glial matter and GM (gray matter) classes.

For the volunteer’s data, manually segmented images (generated by an experienced radio-oncologist) were used to define a ground truth segmentation consisting of five tissue classes (fat, muscle, and skin were treated as a single skin class).

In our experiments, we used BET as the BTSA and a simple algorithm based on thresholding and morphological reconstruction [45] as the NBTSA. For multi-tissue seg-

mentation of brain and non-brain volume, we applied the following MTSAAs: our own BAMS (described in section 3.2), k NN-AMS, FAST (described in section 2.3.2), and k -means (described in section 2.3.3). Hereinafter these four instantiations of the HSA are denoted HSA-BAMS (our proposed method for whole-head segmentation), HSA- k NN-AMS, HSA-FAST, and HSA- k -means.

The evaluation of HSA-BAMS, was done relative to that of three other instantiations of the HSA as well as that of a reference method BET-FAST.

Quantitative results

The qualitative results of synthetic multi-modal MR data (see Fig. 3 in paper B) show that the proposed method HSA-BAMS outperforms the HSA-FAST and HSA- k -means for the skin, skull, muscle, WM, GM, and CSF classification for each noise levels.

The qualitative results of volunteers' data (see Table 1 and 2 in paper B) show that HSA-BAMS performs consistently better than that of all competing methods for the skin, WM, GM, and CSF classification.

Difference in segmentation behaviour

Several multiple comparison tests [46] were performed using both synthetic multi-modal and volunteer's MR data to determine whether there exists a statistically significant difference in segmentation behaviour for each tissue type between the proposed method HSA-BAMS and each of the other methods (see paper B for details).

The tests for synthetic multi-modal MR data with 9% noise level show that HSA-BAMS performs differently ($\alpha = 0.05$) to all other methods for the classification of CSF, GM, WM, fat, and muscle.

The tests for volunteers' MR data provide the evidence that the classification behavior of HSA-BAMS ($\alpha = 0.05$) is different to that of all the other competing methods for the tissues: CSF, WM, GM, and skin.

Qualitative results

The qualitative result of multi-modal MR data with 9% noise level (see Fig. 4 in paper B) shows that the proposed method HSA-BAMS is less sensitive to noise as compared to HSA-FAST and HSA- k -means.

The qualitative results of volunteers' data (see Fig. 6 and Fig. 8 in paper B) show that the proposed method HSA-BAMS has better segmentation of skin, CSF, and GM as compared to that of all other competing methods.

4.4 Indirect evaluation of the proposed method in the context of non-invasive EEG source localization

Electroencephalography (EEG) source localization is a non-invasive tool used to locate the source of epileptic seizures in the brain. It involves the solution of two problems: (1) Forward problem which deals with finding the scalp potentials for the given current sources and (2) Inverse problem which deals with estimating the sources to fit with the given the potential distributions at the scalp electrodes [47]. The accuracy of EEG source localization is based on the quality and fidelity of the patient-specific head conductivity model which in turn based on the accurate segmentation of the patient's head tissues.

Herein, we summarize an indirect empirical evaluation of the proposed segmentation method HSA-BAMS and the two reference segmentation methods, HSA-FAST and BET-FAST, in the context of EEG source localization (see paper C for more details).

The evaluation was performed using (1) synthetic 2D multi-modal MRI head data and synthetic EEG (generated for a prescribed source), and (2) real 3D T1-weighted MRI head data and real EEG data.

Ground truth (GT) consisting of five tissue classes was defined for the synthetic data by merging the connective, fat, muscle and skin tissue classes, and the glial matter and GM (gray matter) tissue classes in the actual labeled data, obtained from the Brainweb. For the real case, a five tissue labeled GT was obtained from a manual segmentation of the volume by an experienced radio-oncologist.

A synthetic EEG was generated by placing a source in the GM of the GT (ground truth) image and calculating the EEG signals from 30 electrodes placed equidistantly on the 2D scalp based on 10/10 system [47].

The real EEG data was obtained by recording the somatosensory evoked potentials (SEPs) on the subjects scalp. These SEPs were generated by stimulating the left wrist median nerve by electric pulses and EEG measurement was done using 61 electrodes based on 10/10 system [12]. The GT for the source was taken to be the expected source region determined independently by an experienced clinician based on neurophysiological knowledge.

The performance of EEG source localization was measured in terms of relative error (RE) between the measured and estimated source potential, localization error (LE) between the actual source and estimated source distance and orientation error (OE) between the actual source and estimated source moment orientation.

A finite element head conductivity model (FEHCM) was constructed from each segmentation method (HSA- BAMS, HSA-HMRF-EM and BET-FAST and GT) using both synthetic and real MR data sets. To solve the EEG source localization problems, a subtraction method was used for modeling the dipole in the forward problem [48] and a modified particle swarm optimization (MPSO) [47] method was applied to solve the inverse problem.

Quantitative results

The quantitative results (see Table II and III in paper C) of both multi-modal synthetic and real T1-weighted MR data for EEG source localization show that HSA-BAMS performs consistently better than all reference methods.

Qualitative results

The qualitative results for both 2D synthetic multi-modal MR data and real MR data (see Fig. 2(e) and Fig. 4 in paper C) show that the source (dipole) position estimated using proposed method HSA-BAMS is similar or closer to the GT source position as compared to that of all reference methods.

Summary of papers and future work

The chapter presents brief summaries of the enclosed papers and a discussion about possible future work.

5.1 Paper A: A Novel Bayesian Approach to Adaptive Mean Shift Segmentation of Brain Images

In this paper we propose a novel adaptive mean shift algorithm for the segmentation of multi-modal MR images of the brain into three tissue types: white matter (WM), gray matter (GM) and cerebrospinal fluid (CSF). The novelty lies in the algorithm for the estimation of the adaptive bandwidth. It is based on a Bayesian approach, we call it BAMS (Bayesian based adaptive mean shift). The accuracy of the proposed BAMS algorithm was evaluated relative to another mean shift algorithm that is based on the k nearest neighbors (k NN) bandwidth estimator and several other existing methods. The segmentation experiments were performed on both multi-modal synthetic (T1-, T2-, PD-weighted) MR data with different levels of noise and real T1-weighted MR data with varying levels of spatial intensity inhomogeneities. The performance of segmentation methods was measured using the Dice and Tanimoto coefficient. The results demonstrate the efficacy and accuracy of proposed BAMS algorithm and that it outperforms the competing methods especially when the noise and spatial intensity inhomogeneities are high.

5.2 Paper B: Automatic Multi-tissue Segmentation of MR Images of the Head Using a Hierarchical Segmentation Approach Incorporating Bayesian-Based Adaptive Mean Shift

In this paper we propose and evaluate a fully automatic method for multi-tissue segmentation in multi-modal MR images of the head. The method is based on a hierarchical segmentation approach (HSA) incorporating Bayesian based adaptive mean shift (BAMS). The segmentation experiments were performed on three data sets: (1) synthetic multi-modal MR data of the human head with differing levels of noise, (2) T1-weighted MR

image of the head of a healthy volunteer and (3) multi-modal MR data (T1- and T2-weighted images) from a second healthy volunteer. The segmentation accuracy of the proposed HSA- BAMS method was evaluated relative to a reference method BET-FAST and three other instantiations of the HSA (HSA- k NN-AMS, HSA-FAST, and HSA- k -means) using the Dice index. Multiple comparison tests (consisting of several McNemar tests) were employed to determine whether there was any statistically significant difference in the voxel-wise classification performance between the proposed and each of the other methods for each tissue type and each data set. The segmentation results for data set 1 show the robustness of proposed method to noise. The results for data sets 2 and 3 demonstrate the accuracy of proposed method and that it consistently outperforms the BET-FAST reference method.

5.3 Paper C: On the Fully Automatic Construction of a Realistic Head Model for EEG Source Localization

In this paper we present an evaluation of a fully automatic method for the construction of realistic finite element head conductivity model (FEHCM) for EEG source localization. The proposed method is based on a hierarchical segmentation approach (HSA) incorporating Bayesian based adaptive mean shift segmentation. The evaluation was performed on (1) 2D synthetic multi-modal (T1-, T2-, PD-weighted) MR data with synthetic EEG data, and (2) real 3D T1-weighted data with real EEG data. The performance of proposed method as well as two reference methods was evaluated in terms of source localization accuracy of their resulting FEHCM. The source localization accuracy was measured in terms of localized error (LE), relative error (RE) of potential and orientation error (OE) between the actual and the estimated source moment. The results show that the proposed method has less LE, RE and OE as compared to other competing methods and that it can be used as a surrogate for manual segmentation for the construction of realistic FEHCM in the application: EEG source localization.

5.4 Future work

Incorporation of more modalities and prior anatomical information

In papers B and C we outlined the less than ideal nature of the real data that was available for the respective studies. Firstly, in both the T1- and T2-weighted gradient echo images the signal intensities for both fat and muscle are heavily attenuated (due to an opposed phase cancelation of signal from both fat and water) which in turn leads to false classification as skull/bone. Secondly, the air and skull/bone tissue have low, overlapping, intensities in the T1- and T2-weighted images which leads to misclassification of the nose and pharynx airways as skull/bone. One possible way to overcome these limitations is to additionally use CT images (they show better contrast for skin/bone tissue). Another, potentially more robust, solution is to use a priori anatomical information; e.g. using probabilistic atlases. We will explore these possibilities in future work.

Classification of abnormal tissues

The proposed methods (in paper A called BAMS whilst in B and C called HSA-BAMS) were applied to segment tissues in multi-modal MR images from healthy subjects with normal anatomy. In the future we plan to extend proposed methods for the segmentation of MR image data containing abnormal brain tissues like sclerotic lesions and tumors. This will likely require additional MRI modalities and possibly also imaging modalities. These can be readily accommodated in our proposed methods.

Novel clustering methods

In future work we aim to investigate contemporary novel clustering methods for brain and whole head tissue segmentation. Two such examples are: quantum clustering and non-linear mean shift clustering. The former approach is based on the quantum mechanics concept where the the Schrödinger equation provides the basis for the clustering of the image [49] and the latter one can be useful for the images where the data points lie on the manifold geometry [50]. For example, MR Diffusion Tensor imaging (DTI).

Bibliography

- [1] B. Hüsing, L. Jäncke, and B. Tag. *Impact Assessment of Neuroimaging*. Institute for Biomedical Engineering, University of Zurich and ETHZ, Zurich, Switzerland, 2005.
- [2] M. Rullmann, A. Anwander, M. Dannhauer, S. Warfield, F. Duffy, and C. Wolter. EEG source analysis of epileptiform activity using a 1 mm anisotropic hexahedra finite element head model. *NeuroImage*, 44(2):399–410, 2009.
- [3] V. Fortunati, R. F. Verhaart, F. van der Lijin, W. J. Niessen, J. F. Veenland, M. M. Paulides, and T. van Walsum. Hyperthermia critical tissues automatic segmentation of head and neck CT images using atlas registration and graphcuts. *In Proceedings of ISBI*, pages 1683–1686, 2012.
- [4] A. Opitz, M. Windhoff, R. Heidemann, R. Turner, and A. Thielscher. How the brain tissue shapes the electric field induced by transcranial magnetic simulation. *NeuroImage*, 58:849–859, 2011.
- [5] K. Wårdell, E. Diczfalusy, and M. Åström. Patient specific modeling and simulation of deep brain stimulation. *In Patient Specific Modeling in Tomorrow's Medicine*, pages 357–378, 2011.
- [6] O. Clatz, H. Delingette, E. Bardinet, D. Dormont, and N. Ayache. Patient specific biomedical model of the brain: application to Parkinson's disease procedure. *In Proceedings of the International Conference on Surgery Simulation and Soft Tissue*, pages 321–331, 2003.
- [7] K. Voo, S. Kumaresan, A. F. Pintar, N. Yoganandan, and A. Sances Jr. Finite element models of the human head. *Med. Biol. Eng. Comput.*, 34:375–381, 1996.
- [8] A. Datta, J. M. Baker, M. Bikson, and J. Fridriksson. Individualized model predicts brain current flow during transcranial direct-current stimulation treatment in responsive stroke patient. *Brain Stimul.*, 4(3):169–174, 2011.
- [9] A. Mayer and H. Greenspan. An adaptive mean-shift framework for MRI brain segmentation. *IEEE Trans. Med. Imag.*, 28(8):1238–1249, 2009.
- [10] A. Brodal. *Neurological Anatomy in Relation to Clinical Medicine*. Oxford Univ. Press, New York, 3rd edition, 1981.

- [11] C. R. Noback, N. L. Strominger, R. J. Demarest, and D. A. Ruggiero. *The Human Nervous System Structure and Function*. Humana Press Inc., Totowa, New Jersey, 6th edition, 2005.
- [12] E. A. Kandel, J. Schwartz, and T. M. Jessell. *Principles of Neural Science*. McGraw-Hill Companies, 4th edition, 2000.
- [13] D. W. McRobbie, E. A. Moore, M. J. Graves, and M. R. Prince. *MRI: From picture to proton*. Cambridge, 2nd edition, 2007.
- [14] R. R. Ernst, G. Bodenhausen, and A. Wokaun. *Principles of Nuclear Magnetic Resonance in one and two dimensions*. Oxford University Press, USA, 1990.
- [15] P. T. Callaghan. *Principles of Nuclear Magnetic Resonance Microscopy*. Oxford University Press, USA, 1993.
- [16] R. A. Pooley. Fundamental physics of MR imaging. *RadioGraphics*, 25:1087–1099, 2005.
- [17] E. M. Haacke, R. W. Brown, M. R. Thompson, and R. Venkatesan. *Magnetic Resonance Imaging: Physical Principles and Sequence Design*. Wiley-Liss, 1999.
- [18] Brainweb: Simultaneous Brain Database. <http://brainweb.bic.mni.mcgill.ca/brainweb/>.
- [19] S. Aja-Fernández, C. Alberola-López, and C. F. Westin. Noise and signal estimation in magnitude MRI and Rician distributed images: a LMMSE approach. *IEEE Trans. on Image Processing*, 17:1383–1398, 2008.
- [20] K. Fukunaga and L. D. Hostetler. The Estimation of the Gradient of a Density Function, with Applications in Pattern Recognition. *IEEE Trans. Information Theory*, 21:32–40, 1975.
- [21] D. Comaniciu and P. Meer. Mean Shift: A robust approach toward feature space analysis. *IEEE Trans. Pattern Analysis Machine Intell.*, 24(5):603–619, 2002.
- [22] Y. Zhang, M. Brady, and S. Smith. Segmentation of brain MR images through a Hidden Markov Random Field Model and the Expectation Maximization algorithm. *IEEE Trans. Med. Imag.*, 20(1):45–57, 2001.
- [23] J. Besag. On the statistical analysis of dirty pictures (with discussion). *Journal of Royal Statist. Soc. B*, 48:259–302, 1986.
- [24] J. B. MacQueen. Some methods for classification and analysis of multivariate observations. *Proceedings of 5th Berkeley Symposium on Mathematical Statistics and Probability*, pages 281–297, 1967.
- [25] J. C. Rajapakse and F. Kruggel. Segmentation of MR images with intensity inhomogeneities. *Image and Vision Computing*, 16(4):165–180, 1998.

- [26] M. Jenkinson, C. F. Beckmann, T. E. Behrens, M. W. Woolrich, and S. M. Smith. FSL. *NeuroImage*, 62:782–790, 2012.
- [27] S. M. Smith. Fast robust automated segmentation. *Human Brain Mapping*, 17(3):143–155, 2002.
- [28] A. Kelemen, G. Szekely, and G. Gerig. Elastic model-based segmentation of 3-D neuroradiological data sets. *IEEE Trans. Med. Imag.*, 18:828–839, 1999.
- [29] A. M. Dale, B. Fischl, and M. I. Sereno. Cortical surface based analysis I. segmentation and surface reconstruction. *NeuroImage*, 9:179–194, 1999.
- [30] D. B. Rash, H. Madasu, G. K. Suresh, and K. G. Sushil. The brain MR image segmentation techniques and use of diagnostic packages. *Acad Radiol.*, 17:658–671, 2010.
- [31] O. M. Alia, R. Mandava, and M. E. Aziz. A hybrid harmony search algorithm for MRI brain segmentation. *Evolutionary Intelligence*, 4:31–49, 2011.
- [32] J. Ghasemi, M. R. K Mollaei, R. Ghaderi, and A. Hojjatoleslami. Brain tissue segmentation based on spatial information fusion by dempster-shafer theory. *Journal of Zhejiang University SCIENCE C*, 13:520–533, 2012.
- [33] J. C. Bezdek, L. O. Hall, and L. P. Clarke. Review of MR image segmentation techniques using pattern recognition. *Med. Phys.*, 20:1033–1048, 1993.
- [34] L. Yi and G. Zhijun. A review of segmentation method for MR image. *In Proc. of IASP*, pages 351–357, 2010.
- [35] L. Clarke, R. Velthuizen, S. Phuphanich, J. Schellenberg, J. Arrington, and M. Silbiger. MRI: stability of three supervised segmentation techniques. *Magnetic Resonance Imaging*, pages 95–106, 1993.
- [36] K. Van Leemput, F. Maes, D. Vandeurmeulen, and P. Suetens. Automated model-based tissue classification of MR images of the brain. *IEEE Trans. Med. Imag.*, 18(10):897–908, 1999.
- [37] H. Greenspan, A. Ruf, and J. Goldberger. Constrained Gaussian mixture model framework for automatic segmentation of MR brain images. *IEEE Trans. Med. Imag.*, 25(9):1233–1245, 2006.
- [38] J. L. Marroquin, B. C. Vemuri, S. Botello, and F. Calderon. An accurate and efficient Bayesian method for automatic segmentation of brain MRI. *IEEE Trans. Med. Imag.*, 21(8):934–944, 2002.
- [39] R. J. Jimenez-Alaniz, Mauricio Pohl-Alfaro, V. Medina-Bafluelos, and Oscar Yáñez Suárez. Segmenting brain MRI using adaptive mean shift. *Annual International Conference of the IEEE Engineering in Medicine and Biology Society*, pages 3114–3117, 2006.

-
- [40] A. G. Bors and N. Nasios. Kernel bandwidth estimation for nonparametric modeling. *IEEE Trans. SMC*, 39:1543–1555, 2009.
- [41] Internet Brain Segmentation Repository Center for Morphometric Analysis. www.cma.mgh.harvard.edu/ibsr.
- [42] P. Dokládal, I. Bloch, M. Couprie, D. Ruijters, R. Urtasun, and L. Garnero. Topologically controlled segmentation of 3D Magnetic Resonance images of the head by using morphological operators. *Pattern Recognition*, 36:2463–2478, 2003.
- [43] U. Amato, M. Larobina, A. Antoniadis, and B. Alfano. Segmentation of Magnetic Resonance brain images through discriminant analysis. *Journal of Neuroscience Methods*, 131:65–74, 2003.
- [44] Z. A. Acar and S. Makeig. Neuroelectromagnetic forward modeling toolbox. *Journal of Neuroscience Methods*, 190:258–270, 2010.
- [45] P. Soille. Morphological image analysis: Principles and applications. *Springer-Verlag*, 4(3):173–174, 1999.
- [46] T. G. Dietterich. Approximate statistical tests for comparing supervised classification learning algorithms. *Neural Comput.*, 10:1895–1923, 1998.
- [47] Y. Shirvany, F. Edelvik, S. Jakobsson, A. Hedstörn, Q. Mahmood, A. Chodorowski, and M. Persson. Non-invasive EEG source localization with Particle Swarm Optimization: Clinical Test. In *Proc. of 34th Annual Int. Conf. EMBC*, pages 6232–6235, 2012.
- [48] F. Edelvik, B. Andersson, S. Jakobsson, S. Larsson, M. Persson, and Y. Shirvany. An improved method for dipole modeling in EEG based source localization. In *Proc. of IFMBE*, pages 146–149, 2009.
- [49] D. Horn and A. Gottlieb. Algorithm for data clustering in pattern recognition problems based on quantum mechanics. *Physical Review Letters*, 88:18702–18704, 2002.
- [50] R. Subbarao and P. Meer. Nonlinear mean shift over Riemannian manifolds. *Int. J. Comput. Vision*, 84:1–20, 2009.